Accurate Lifetime Measurements of Superdeformed Bands in $A \sim 80$ Nuclei

F. Lerma,[1] M. Devlin,[1,*] D. R. LaFosse,[1,†] D. G. Sarantites,[1] R. Wyss,[2] C. Baktash,[3] R. M. Clark,[4] I. Y. Lee,[4] A. O. Macchiavelli,[4] R. W. MacLeod,[4] D. Soltysik,[5] and S. L. Tabor[5]

[1]*Chemistry Department, Washington University, St. Louis, Missouri 63130*
[2]*KTH, Department of Physics-Frescati, Frescativägen 24, S-104 05, Stockholm*
[3]*Physics Division, Oak Ridge National Laboratory, Oak Ridge, Tennessee 37830*
[4]*Nuclear Science Division, Lawrence Berkeley National Laboratory, Berkeley, California 94720*
[5]*Department of Physics, Florida State University, Tallahassee, Florida 32306*

(Received 10 May 1999)

Comparative measurements of the lifetimes of yrast superdeformed (SD) states in $^{80-83}$Sr, ^{83}Y, and ^{84}Zr have been performed using the Doppler-shift attenuation method. Thus, the transition quadrupole moments (Q_t) of these structures have been determined accurately. The yrast SD bands in $^{80-83}$Sr possess $Q_t \sim 3.5\ e$ b, while the ^{83}Y and ^{84}Zr cases display $Q_t = 4.4\ e$ b and 5.6 e b, respectively. Intruder orbital assignments based on these results demonstrate a previously unnoticed transition in the structure of the SD bands when the proton number changes from $Z = 38$ to $Z \geq 39$.

PACS numbers: 21.10.Tg, 21.10.Re, 21.60.–n, 27.50.+e

Since the discovery of a discrete superdeformed (SD) band in ^{83}Sr [1,2], highly improved detection capabilities have allowed the study of a multitude of SD bands in nuclei of mass ~80. Thus, earlier predictions of SD shell gaps at neutron number $N = 44$, and proton numbers $Z = 38$–40 have been confirmed. From those experimental investigations, SD bands in $A \sim 80$ nuclei have been characterized as largely deformed prolate structures ($\beta_2 \sim 0.5$) due to their high spin nature, large dynamical moments of inertia ($\mathcal{J}^{(2)}$), and in some cases from measured [3–8] transition quadrupole moments (Q_t). However, large experimental uncertainties limited the accuracy of previous lifetime measurements, hampering clear comparisons of the deformations of the SD bands in those nuclei. Consequently, stringent tests of theoretical calculations, and well-defined trends in the deformation of SD bands across the $A \sim 80$ nuclei, have not been previously possible.

In this work, we present the results of an experiment aimed at measuring comparatively the transition quadrupole moments of the SD bands in $^{80-83}$Sr, ^{83}Y, and ^{84}Zr. The Q_t values are deduced from the measured lifetimes of the SD states via a target thickness, and target-backing-thickness induced Doppler-shift attenuation method, similar to that described in Ref. [9]. The reduced systematic and statistical errors in the present Q_t values allow accurate comparisons from which the evolution of superdeformation is demonstrated as a function of $N = 42$–45 and $Z = 38$–40. A detailed examination of the intruder orbital assignments is given.

The experiment was performed at the 88" Cyclotron at the Lawrence Berkeley National Laboratory. A single 530 μg/cm^2 ^{58}Ni target foil backed with 3.2 mg/cm^2 of gold was used in two separate reactions. In the first reaction, the target was bombarded with a ^{28}Si beam at 130 MeV, populating high spin states in ^{80,82}Sr, and ^{83}Y, via the $\alpha 2p$, $4p$, and $3p$ fusion-evaporation exit channels, respectively. In the second reaction, a ^{29}Si beam at 130 MeV was used to populate high-spin states in ^{81,83}Sr and ^{84}Zr via the $\alpha 2p$, $4p$, and $2pn$ exit channels, respectively. The γ rays were detected by the Gammasphere array, which consisted of 100 hyperpure Ge detectors fitted with bismuth germanate (BGO) Compton suppressors, and the evaporated charged particles were detected by the Microball charged-particle detector array [10]. Each reaction was run for two days, yielding $\sim 9 \times 10^8$ events per reaction. The hevimet absorbers were removed during the experiment to obtain total γ-ray energy (H_γ), and γ fold information per event [11], and the event trigger was set to accept events with clean γ fold equal to 4 and higher. The Microball provided good charged particle identification, which was used to sort the data into individual exit channels. Residual contaminants resulting from unidentified protons, α particles, and neutrons were sharply reduced by placing gates on H_γ and excitation energy ($E^* = \text{const} - \Sigma$ particle energies) [12].

The γ-ray energy spectra of the decays from the recoiling nuclei display large Doppler shifts which decrease as a function of the slowing of the nuclei in the target and backing, and which become constant upon the escape from the Au backing. Therefore, to sharpen the E_γ spectra of the SD bands, the energies of the charged particles detected with the Microball were used to reconstruct the momenta [and, consequently, the initial recoil velocity (β_0)] of the recoiling nuclei on an event-by-event basis. These momenta were then scaled arbitrarily as a function of E_γ, to simulate the varying velocity distributions of the recoiling nuclei in the target (during the decays of the SD bands), and used to apply a precise Doppler-shift correction (β_{app}) to the γ-ray energies.

The resultant, Doppler-shift corrected E_γ from events in individual exit channels, were sorted into seven E_γ-E_γ matrices, to measure the residual centroid shifts of the SD bands. Each matrix contained coincidences of detectors in a narrow angular segment (relative to the beam axis)

and any other detector. The individual angular segments consisted of groups of rings of detectors in the Gammasphere array at average angles $\overline{\theta} = 29.9°$, 52.9°, 74.3°, 90.0°, 105.1°, 127.1°, and 150.1°. The matrices were gated on the energies of in-band transitions of the SD bands, and one-dimensional spectra were projected onto the axis containing counts from the angular segment, $\overline{\theta}$. The centroids of the SD band transitions (E_γ) were measured in the resultant spectra. Subsequently, a residual Doppler shift ($\beta_{\rm res}$) was fitted to the seven ($E_\gamma, \overline{\theta}$) pairs (for each transition in the SD bands), using the expression $E_\gamma = E_\gamma^0\sqrt{1 - \beta_{\rm res}^2}/[1 - \beta_{\rm res}\cos(\overline{\theta})]$, by a least-squares procedure. The velocities from the residual $\beta_{\rm res}$ and applied Doppler shifts $\beta_{\rm app}$ of individual transitions add relativistically to obtain an average recoil velocity β, which is expressed as a fraction of the initial recoil velocity, $\beta/\beta_0 \equiv F(\tau)$. A one dimensional spectrum single gated on the SD band in ^{84}Zr is shown in Fig. 1(a). Spectra projected from separate angular segments of detectors are shown in the insets, Figs. 1(b) and 1(c).

The average Q_t values of the SD bands were determined by fitting the fractional Doppler shifts [$F(\tau)$] of each SD band, with calculated values, using the Doppler-shift attenuation method (with a model calculation procedure from Ref. [13]) described in Refs. [3,5,9]. In this method, the decay times of the states in the SD bands are related to the velocity of the recoiling nuclei as they slow down in the target. Side feeding was modeled based on measured intensity patterns, and a constant Q_t was fitted to all levels in-band and those in the side-feeding cascades, as developed by Lee [13], and further discussed in Ref. [14]. Thus, side-feeding times were assumed to be equal to those of preceding in-band transitions.

Absolute values obtained from this method contain systematic errors which result from the electronic and nuclear stopping power estimates [15] that are used to calculate the slowing of the recoiling nuclei in the target and backing. However, for the time scales, and therefore, the velocities involved in the decay of the SD states, the electronic stopping, which is well known, dominates. Thus, large systematic errors due to nuclear stopping when the recoiling species slow down in the target and Au backing are reduced, and accurate comparisons of the extracted values can be made for residual nuclei of different Z.

The $F(\tau)$ of the yrast SD bands in $^{80-83}$Sr, ^{83}Y, and ^{84}Zr, obtained in this work are plotted as solid circles in Fig. 2. Similarly, the $F(\tau)$ of the yrast SD band in ^{81}Sr from a previous thin-target experiment [5], are shown as open circles, for comparison. The $^{80-83}$Sr data from the backed target experiment span the largest ranges in $F(\tau)$, and consequently, demonstrate an enhanced sensitivity to the lifetimes of those SD bands. In contrast, the fitted $F(\tau)$ of the SD bands in ^{83}Y and ^{84}Zr, and the fit to the yrast SD band in ^{81}Sr (from Ref. [5]) demonstrate reduced ranges in $F(\tau)$, which are due to the shorter decay times of the SD bands in ^{83}Y and ^{84}Zr, and to the absence of the Au backing in the thin target example, respectively. The Q_t values corresponding to the calculated $F(\tau)$ profiles (shown in Fig. 2) are summarized in Table I.

The Q_t values of the SD bands in $^{80-83}$Sr, ^{83}Y, and ^{84}Zr from this experiment, from recent works [3,5,6,8], and from previous intruder-orbital configuration assignments [1–3,5,6,8,16–18] are shown in Fig. 3(a), for the $Z = 38$ isotopes, and in Fig. 3(b), for the $N = 44$ isotones. Previous intruder orbital assignments predicted an increase in Q_t of the SD bands across the $Z = 38$ isotopes ($^{80-83}$Sr), and the experimental evidence had suggested a partial

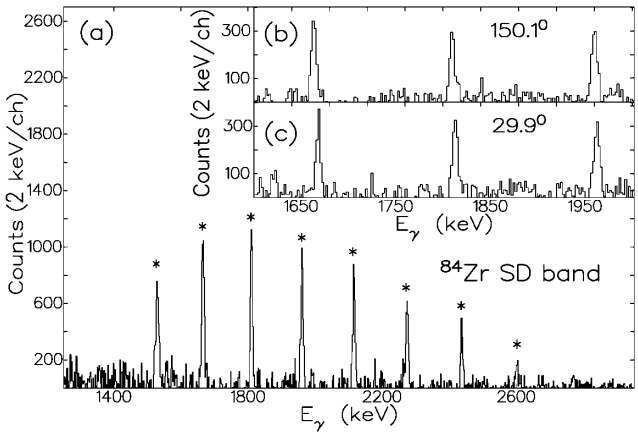

FIG. 1. A spectrum resulting from the sums of clean single gates (indicated by asterisks) on in-band transitions of the SD band in ^{84}Zr is shown in panel (a). Insets (b) and (c) contain spectra single gated on the SD band in ^{84}Zr, projected from groups of detectors at narrow angular segments, at 150.1° and 29.9°, respectively.

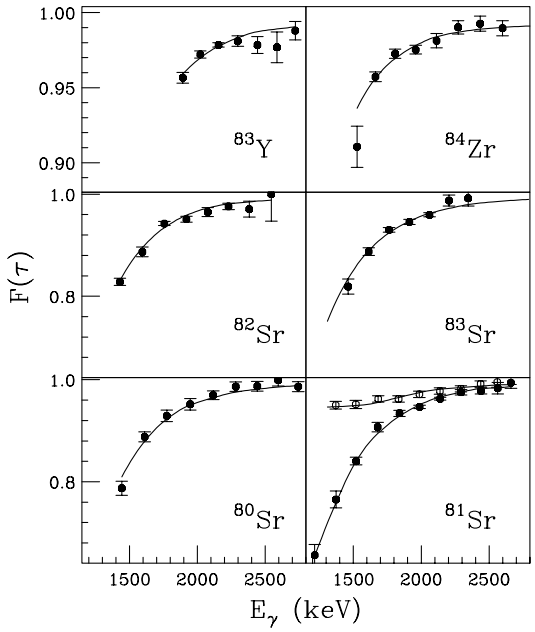

FIG. 2. Measured (fitted) fractional Doppler-shifts $F(\tau)$ of the yrast SD bands in $^{80-83}$Sr, ^{83}Y, and ^{84}Zr are shown as solid circles (solid lines). Values obtained in a previous work [5] for the yrast SD band in ^{81}Sr, using a thin target, are displayed as open circles, for comparison.

TABLE I. Previous SD configuration assignments [1–3,5,6,8,16–18], new SD configuration assignments, newly calculated values ($\beta_2^{\rm th}, \gamma^{\rm th}, Q_t^{\rm th}$), and newly fitted $Q_t^{\rm exp}$.

Structure	Config. Previous	Config. New	$\beta_2^{\rm th}, \gamma^{\rm th}$ New	$Q_t^{\rm th}$ New (e b)	$Q_t^{\rm exp}$ (e b)
^{80}Sr SD1	$\nu 5^1 \pi 5^0$	$\nu 5^1 \pi 5^0$	$0.45, 2.0^0$	4.3	$3.42^{+0.26}_{-0.23}$
^{81}Sr SD1	$\nu 5^1 \pi 5^0$	$\nu 5^1 \pi 5^0$	$0.46, 1.2^0$	4.4	$3.30^{+0.18}_{-0.16}$
^{82}Sr	$\nu 5^2 \pi 5^1$	$\nu 5^1 \pi 5^0$	$0.50, 6.0^0$	4.5	$3.54^{+0.15}_{-0.14}$
^{83}Sr	$\nu 5^3 \pi 5^1$	$\nu 5^1 \pi 5^0$	$0.43, 13.0^0$	3.5	$3.60^{+0.20}_{-0.18}$
^{83}Y SD1	$\nu 5^2 \pi 5^1$	$\nu 5^2 \pi 5^1$	$0.54, 3.2^0$	5.7	$4.4^{+0.7}_{-0.7}$
^{84}Zr	$\nu 5^2 \pi 5^1$	$\nu 5^2 \pi 5^1$	$0.56, 3.5^0$	6.1	$5.6^{+0.6}_{-0.5}$

confirmation of that trend. Likewise, for the SD bands in the $N = 44$ isotones (^{82}Sr, ^{83}Y, and ^{84}Zr), calculations indicated large deformations, which were in satisfactory agreement with experimental values [3,6] (within the large experimental uncertainties). However, the present results provide more accurate comparisons revealing trends that differ significantly from earlier interpretations. The yrast SD bands in $^{80-83}$Sr possess similar transition quadrupole moments, $Q_t \sim 3.5$ e b, and the SD bands in ^{83}Y and ^{84}Zr have larger Q_t values ~ 5 e b.

In order to clarify the structure of these SD bands, extended total routhian surface calculations have been performed [19]. In these Woods-Saxon Strutinsky-type calculations, the shape of the potential is minimized with respect to deformation parameters β_2, β_4, and γ. The lowest lying configurations of given signature and parity are separately calculated self-consistently in order to address polarization effects in an accurate manner [20]. The moment of inertia is then calculated from the expectation value of $\langle I_x \rangle$ at the minimum of the potential for the different configurations. Similarly, the quadrupole moment is calculated from the expectation value of the Q_{20} and Q_{22} operator at the minimum at each frequency. The final selection of the configurations that are assigned to the SD bands are based on the criteria that they should be yrast or close to yrast in the frequency range considered, and that the calculated $\mathcal{J}^{(2)}$ and Q_t should be close to the measured values.

The calculated Q_t values of the selected configurations are shown in Fig. 3. As can be seen the Q_t values from the new calculations reproduce well the variations in the relative values of the SD bands in $^{80-82}$Sr, ^{83}Y, and ^{84}Zr, thus suggesting that the observed differences arise from a systematic offset of $\sim$15%. The drop in the calculated Q_t value for ^{83}Sr is explained by a significant deviation of the deformation parameters from the prolate collective axis towards positive γ values. Specifically, with increasing neutron number, the SD states of the Sr isotopes become γ-soft, implying that the calculated values may become less accurate. In Fig. 4, the newly calculated and experimentally deduced $\mathcal{J}^{(2)}$ of the SD bands in $^{80-83}$Sr, ^{83}Y, and ^{84}Zr are compared. The slight scatter observed in

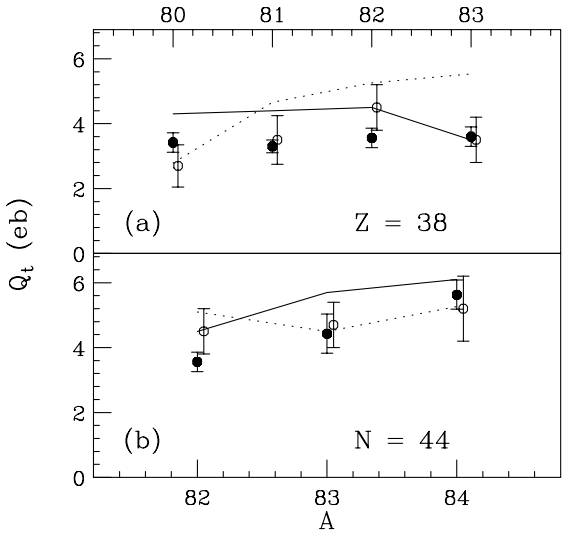

FIG. 3. The average transition quadrupole moments obtained for the yrast SD bands in $^{80-83}$Sr are shown in panel (a), and those values obtained for the ^{82}Sr, ^{83}Y, and ^{84}Zr cases are displayed in panel (b). Values obtained from the new experiment are plotted as solid circles. Values from previous works [3,5,6,8] are shown as open circles (displaced by 0.05 units in the x axis for clarity). Newly (previously) calculated values are shown, joined by solid (dotted) lines.

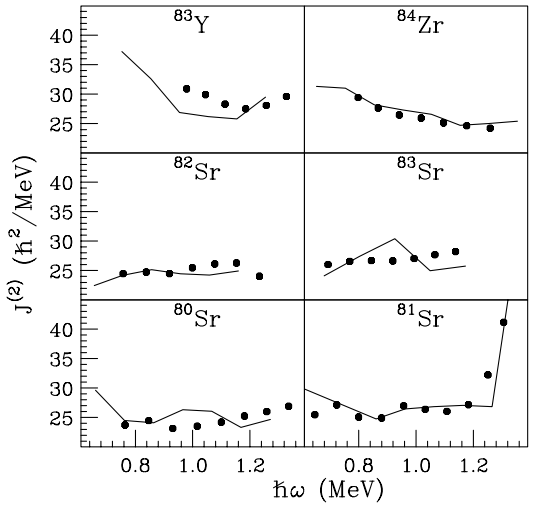

FIG. 4. The dynamic moments of inertia of the yrast SD bands in $^{80-83}$Sr, ^{83}Y, and ^{84}Zr are compared; the measured values are shown as solid circles, and the newly calculated values are joined by solid lines.

the calculated moments of inertia of the $^{80-83}$Sr isotopes is a result of the soft routhian surfaces in those nuclei. Nevertheless, in general, these comparisons show that the new intruder orbital assignments are in very good agreement with the experimental properties of these SD bands.

In this interpretation, the yrast SD bands in $^{80-83}$Sr arise from $\nu 5^1 \pi 5^0$ configurations, whereas the ^{83}Y and ^{84}Zr yrast SD bands are assigned $\nu 5^2 \pi 5^1$ configurations. In the case of ^{84}Zr an additional proton occupies the [431]1/2 Nilsson intruder orbit, also originating from the shell above. Thus, a systematic correspondence exists between the number of $\nu h_{11/2}$ and $\pi h_{11/2}$ excitations and the measured relative Q_t of the six SD bands; the SD bands in $^{80-83}$Sr possess smaller Q_t values and one $\nu h_{11/2}$ excitation, and the SD bands in ^{83}Y and ^{84}Zr show larger Q_t values, and both possess 1 $\pi h_{11/2}$, and 2 $\nu h_{11/2}$ excitations. These results are summarized in Table I. The distinctly fewer $h_{11/2}$ excitations in the configurations of the SD bands in ^{82,83}Sr in this work, vs those in previous works [1,2,6,17] may be understood as follows.

In our calculations, the $N = Z = 38$ gap at highly deformed shapes $\beta_2 \approx 0.4$ is stable, up to the highest frequencies. Hence, promotions of protons into the high-j intruder orbitals from the $N = 5$ shell are not energetically favorable for the $^{80-83}$Sr isotopes. The present Q_t measurement confirms the calculated stability of the $Z = 38$ gap, that effectively prevents the shape of the Sr isotopes to really become superdeformed. Hence the SD bands in $^{80-83}$Sr are interpreted as well-deformed prolate rotors ($\beta_2 \lesssim 0.5$), with a triaxial character in the ^{82,83}Sr cases. In the presence of pairing correlations, a pronounced $\nu h_{11/2}$ alignment is expected in the Sr isotopes, which would result in a large bump in the $\mathcal{J}^{(2)}$. Such a bump is certainly absent in the data, thus hinting at an error in the earlier configuration assignments [1,2,6,17]. This also shows that pairing correlations are crucial for a complete understanding of the structure of even nuclei at high angular momenta [21]. Notably, the sharp rise in the $\mathcal{J}^{(2)}$ in ^{81}Sr reflects the occupation of the first proton $h_{11/2}$ intruder orbital, resulting in a major shape change in the calculations.

There is a major difference in the structure of the SD bands when the proton number changes from $Z = 38$ to $Z = 39$, which was unnoticed previously. A proton $h_{11/2}$ excitation is energetically accessible, and the lack of a pronounced shell structure at SD shapes with $Z = 39$–41 causes the equilibrium deformation to be further determined by the shell gaps of the neutrons. For the neutrons, a magic gap at SD shape $\beta_2 \approx 0.6$ is obtained at $N = 44$, which is stable over a large frequency range, resulting in the occupation of one pair of $h_{11/2}$ neutrons. For $N = 43$, a similar gap in the single particle spectrum occurs, at a smaller deformation, where only a single $h_{11/2}$ neutron is occupied. Therefore, passing from $N = 43$ to $N = 44$ may result in an increase of the calculated Q_t, of ~ 0.6 e b for the yrast SD bands in ^{83,84}Zr, related to the change in structure of $\nu 5^1$ to $\nu 5^2$. Therefore, the SD bands in ^{83}Y and ^{84}Zr have greater calculated quadrupole deformations ($\beta_2 \sim 0.55$) and only a modest triaxiality.

In summary, the average transition quadrupole moments of the SD bands in $^{80-83}$Sr, ^{83}Y, and ^{84}Zr have been measured under nearly identical experimental conditions. Thus, accurate trends in the relative Q_t values of these SD bands are obtained for the first time. The SD bands in $^{80-83}$Sr possess moderate Q_t values ~ 3.5 e b, and the SD bands in ^{83}Y and ^{84}Zr have larger values $Q_t \sim 5$ e b. Comparisons with Q_t values from previous intruder-orbital assignments show large discrepancies, which are addressed with new theoretical calculations. As a result, different configurations are assigned to the ^{82,83}Sr cases, in which fewer high-j ($\nu h_{11/2}$ and $\pi h_{11/2}$) intruder orbitals are occupied. Thus, there is a major change in the SD structures from $Z = 38$ to $Z = 39$, which is interpreted in terms of a stable proton shell gap at high frequencies.

This work is supported in part by the U.S. D.O.E. under Grant No. DE-FG02-88ER-40406 (W. U.), Contracts No. DE-AC03-76SF00098 (LBNL) and No. DE-AC05-96OR22464 (ORNL); by the National Science Foundation (FSU), and by the Swedish Natural Science Research Council.

*Current address: LANSCE-3, Los Alamos National Laboratory, Los Alamos, New Mexico 87545.
†Current address: Department of Physics and Astronomy, SUNY at Stony Brook, Stony Brook, NY 11794.

[1] C. Baktash *et al.*, Phys. Rev. Lett. **74**, 1946 (1995).
[2] D. R. LaFosse *et al.*, Phys. Lett. B **354**, 34 (1995).
[3] H.-Q. Jin *et al.*, Phys. Rev. Lett. **75**, 1471 (1995).
[4] D. G. Sarantites *et al.*, Phys. Rev. C **57**, 1 (1998).
[5] M. Devlin *et al.*, Phys. Lett. B **415**, 328 (1997).
[6] C.-H. Yu *et al.*, Phys. Rev. C **57**, 113 (1998).
[7] D. Rudolph *et al.*, Phys. Lett. B **389**, 463 (1996).
[8] H.-Q. Jin *et al.* (to be published).
[9] B. Cederwall *et al.*, Nucl. Instrum. Methods Phys. Res., Sect. A **354**, 591 (1995).
[10] D. G. Sarantites *et al.*, Nucl. Instrum. Methods Phys. Res., Sect. A **381**, 418 (1996).
[11] M. Devlin *et al.*, Nucl. Instrum. Methods Phys. Res., Sect. A **383**, 506 (1996).
[12] C. E. Svensson *et al.*, Nucl. Instrum. Methods Phys. Res., Sect. A **396**, 228 (1996).
[13] I. Y. Lee (private communication).
[14] F. Lerma *et al.* (to be published).
[15] J. F. Ziegler, J. P. Biersack, and U. Littmark, *The Stopping and Ranges of Ions in Matter* (Pergamon, London, 1985), Vol. 1.
[16] W. Nazarewicz *et al.*, Nucl. Phys. A **435**, 397 (1985).
[17] A. G. Smith *et al.*, Phys. Lett. B **355**, 32 (1995).
[18] F. Cristancho *et al.*, Phys. Lett. B **357**, 281 (1995).
[19] W. Satuła and R. Wyss, Phys. Rev. C **50**, 2888 (1994); W. Satuła and R. Wyss, Phys. Scr. **T56**, 159 (1995).
[20] R. Wyss and W. Satuła, Phys. Lett. B **351**, 393 (1995).
[21] W. Nazarewicz, R. Wyss, and A. Johnson, Phys. Lett. B **225**, 208 (1988).